

Article

Removal of Pb^{2+} from Water by Synthesized Tannin Resins from Invasive South African Trees

Bamidele J. Okoli ^{1,*} , Patience M. Shilowa ¹ , Gabriel O. Anyanwu ²  and Johannes S. Modise ¹

¹ Institute of Chemical and Biotechnology, Vaal University of Technology, Southern Gauteng Science and Technology Park, Private Bag X021, Vanderbijlpark 1911, South Africa; patience.shilowa@sasol.com (P.M.S.); joe@vut.ac.za (J.S.M.)

² Department of Biochemistry, Bingham University, Karu P.M.B 005, Nigeria; gabrielanyanwu@binghamuni.edu.ng

* Correspondence: okolibj@binghamuni.edu.ng

Received: 18 March 2018; Accepted: 20 April 2018; Published: 17 May 2018



Abstract: Contamination of water by Pb^{2+} and the threat of invasive vegetation affects the quality and quantity of water accessible to all life forms and has become a primary concern to South Africa and the world at large. This paper synthesized, characterized, and evaluated the resins from tannin-rich invasive *Acacia* species as an environmentally benign Pb^{2+} adsorbent. The analysis of the pore volume and surface area of the resins reveals a small pore dimension of 9×10^{-3} cc/g and large surface area (2.31–8.65 m²/g), presenting suitable physical parameters for adsorption of Pb^{2+} . Langmuir model offers the best correlation data at pH 6 with maximum monolayer coverage capacity of 189.30, 105.70 and 98.82 mg/g for silver, black and green wattle tannin resins in aqueous solutions, respectively. The kinetic data suitably fits into a pseudo-second-order model, with the Dubinin–Radushkevich adsorption energy (E) ≤ 7.07 KJ/mol and intra-particle diffusion model confirming an associated physisorption process within the bio-sorption system. The thermogravimetric analysis (TGA) and Fourier-transform infrared (FT-IR) data of the resins were informative of the high thermal stability and chelating functionality such as -OH and -NH₂ responsible for the removal of Pb^{2+} . All the resins showed good adsorption characteristics while silver wattle tannin resin has the best adsorption capacity compared to black and green wattle tannin resins. This study provides a prototype adsorbent from invasive plants for the removal of Pb^{2+} in water.

Keywords: *Acacia* species; adsorption; cross-linking; diffractograms; micrograph; thermogravimetric analysis

1. Introduction

The quality of water can be affected by several anthropogenic activities [1]. In South Africa, Pb^{2+} is the primary source of water pollution resulting from mining, textile, battery, leather, and electro coatings industries. Pb^{2+} contamination is considered a priority pollutant because it is highly toxic to humans and aquatic organisms even at low concentrations [2]. It is also able to bio-accumulate and bio-persist in the environment [3]. In South Africa, the availability of water is a significant concern due to changing rainfall patterns. South Africa is now considered to be a water-scarce country [4]. Improving water conservation, water quality and water-use efficiency is a key national priority [5]. The availability of water is threatened by the encroachment of a considerable number of non-native species. This is because of the high biomass and evapotranspiration rates associated with invasive alien plants that arise because of their greater height, root depth and senescence, compared to the native species that they replace [6], consequently causing a decrease in both surface runoff water and

groundwater recharge [7]. For example, tannin-rich *Acacia* species have been classified as a noxious “category 2 invasive weed”, because of its impacts on the surface and groundwater reserves [8,9]. Hence, a prevention strategy has been considered and established, which includes regular survey, management, and prevention of alien vegetation. However, there may be a use for some alien tree species such as *Acacia* that are rich in tannins.

Adsorption studies have shown that materials such as activated carbon, phosphate and natural phosphate have been applied for the removal of heavy metals from wastewater on a commercial scale, but these adsorbents have been certified to have limited application for the removal of Pb^{2+} , asbestos, cysts, and coliform [10–12], hence the non-application of these adsorbents as a primary filter in water treatment. Recent studies have shown that heavy metals can be removed from water and wastewater by efficient, low-cost remediation plant materials and natural tannin adsorbent [13–15]. Zhao et al. [16] and Binaeian et al. [17] reported that fabricated tannin-based dithiocarbamate and hexagonal mesoporous silicate biosorbents are efficient in the removal of Ni^{2+} and anionic dye from aqueous solutions, respectively. Other studies have supported the influence of tannin-rich plants on the biological availability of metal ions by chelation [18,19], but the high solubility of tannin in aqueous solution has limited its direct application as a biosorbent, although several methods such as impregnation of tannin on chitin [20], binding of tannin to aminohexyl cellulose and collagen-fiber [21,22] have been reported for the immobilization of tannin in aqueous solutions with suitable adsorption capacity for toxic metals.

This work focuses on the preparation of a green, cost-effective and environmentally benign immobilized tannin resin adsorbent with enhanced functionality and thermal stability for the remediation of water contaminated by Pb^{2+} . The choice of the *Acacia* species in this study was based on our findings [23], which indicate that the stem barks of this species can hyper-accumulate heavy metals due to the significantly large tannin content.

2. Experimental

2.1. Collection, Authentication and Pre-Extraction Treatment

Stem bark of *Acacia mearnsii* (Black wattle), *A. decurrens* (Green wattle) and *A. dealbata* (Silver wattle) were collected in summer from Ratanda (26.5535° S, 28.3199° E), Hindenburg, South Africa. Voucher specimen number: 17,062, 17,063 and 17,065 were deposited for *A. mearnsii*, *A. decurrens*, and *A. dealbata*, respectively, at the National Biodiversity Institute, Pretoria, South Africa. The stem bark was air dried at ambient temperature for three months.

2.2. Sequential Extraction of Tannin

The dried stem bark of each of the three *Acacia* species were pulverized using an S4 hammer mill (Drotsky, South Africa) and sequentially macerated with hexane, chloroform, ethyl acetate, methanol, and water at room temperature for a week. The water-soluble fractions of hexane, chloroform and ethyl acetate were combined with the aqueous extract and then freeze-dried at 218 K under vacuum (Figure 1). The solid tannins were finally stored in a desiccator containing anhydrous sodium sulfate.

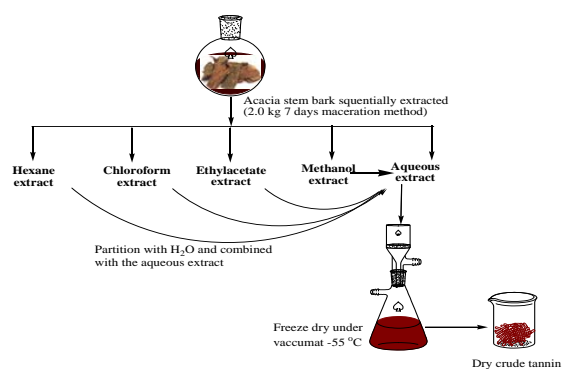


Figure 1. Sequential Extraction of Tannin from the *Acacia* Stem Bark.

2.3. Estimation of Tannin in the Aqueous Fraction

The presence of tannin was confirmed by adding 3 drops of 0.1% FeCl_3 to 1 mL of the aqueous fraction [24]. The Folin-Ciocalteu method was used to quantify the total tannin content [25], by preparing a 100 mg/mL stock solution of tannic acid and making serial dilutions. The amount of tannin in 0.5 mL aliquot of the water fraction was estimated by measuring the absorbance at 700 nm for both standard and test samples on a Cary 60 UV-Vis Spectrophotometer (Agilent, Santa Clara, CA, USA). The tannin content was expressed in mg/g of extract.

2.4. Synthesis of Tannin-Resin

About 25 g of dry extracted tannin powder was dissolved in ammonia solution (13.3 N, 156.25 mL) at room temperature, and cross-linked with benzaldehyde (37 wt %, 201.13 mL). The mixture was stirred at room temperature for 5 min, filtered through filter paper (No. 2) and the residue collected as a dark material (Figure 2).

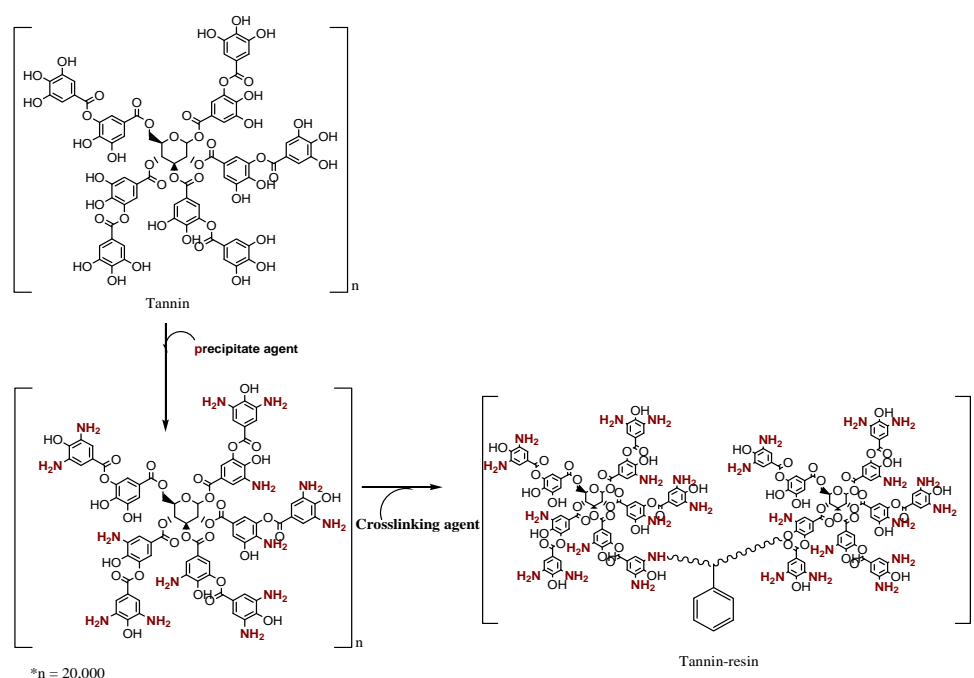


Figure 2. Preparation of Resin.

To the dark material, 150 mL of deionized water was added, heated at 343 K for 3 h, filtered using a vacuum pump, and 100 mL of 0.1 mol/dm³ nitric acid was added to the residue while stirring for 30 min. Finally, the water-insoluble material was allowed to cure at 353 K [26], dried, pulverized and sieved to obtain molecular size fraction of +100 μm using the American Society for Testing and Materials (ASTM) standard sieve.

2.5. Characterisation of Tannins and Resins

The thermal properties were monitored on a thermogravimetric analyzer (Perkin Elmer, Waltham, MA, USA) operated at a temperature range of 303–1173 K at a heating rate of 283 K/min under a nitrogen atmosphere. The functional group composition of the resins was determined on FT-IR (PerkinElmer Spectrum 400, Waltham, MA, USA) scanned between 4000 and 500 cm^{-1} . The resin topography recorded by an X-Ray diffractometer (ZEISS Sigma 300, Oberkochen, Germany), while the surface morphology was scanned with an emission electron microscope (JSM-7500F, Waltham, MA, USA). The pore volume and surface area were estimated using a Brunauer–Emmett–Teller analyzer (Nova 3200e, Boynton Beach, FL, USA).

2.6. Batch Adsorption Study

The sorption isotherms and kinetics were studied using batch adsorption method. A 1000 ppm stock solution of Pb^{2+} was prepared by dissolving 1.6 g of $\text{Pb}(\text{NO}_3)_2$ in 1000 mL of deionized water. The effect of pH on the adsorption pattern of the resins was investigated by adding about 0.05 g resin into 100 ppm $\text{Pb}(\text{NO}_3)_2$ solution in a 100 mL volumetric flask. A solution of 0.1 mol/L HNO_3 and NaOH was added in drop for pH adjustment. The temperature of the Pb^{2+} solution was adjusted at an interval of 10 K between (283–360 K) to evaluate the effect of temperature on the adsorption behaviour of the resins. After centrifuging with an OHAUS centrifuge (Frontier 5816R, Greifensee, Switzerland), the Pb^{2+} concentration was analysed using an inductively coupled plasma spectrometer (ICP-OES PerkinElmer, Billerica, MA, USA). The adsorption capacity q_t (mg/g) of the resins was computed as shown in Equation (1):

$$q_t = \frac{(C_i - C_t)V}{m} \quad (1)$$

where V : volume of sorbent (L), m : the mass of resin (g), C_i and C_t are Pb^{2+} concentrations (mg/L) at the initial and time, respectively.

Batch equilibrium tests were also conducted to determine the adsorption of Pb^{2+} onto the resins at equilibrium. The equilibrium concentration was determined using the following formula Equation (2):

$$q_e = \frac{(C_i - C_e)V}{m} \quad (2)$$

where q_e is the quantity of Pb^{2+} adsorbed at equilibrium (mg/g), and C_e (mg/L) is the equilibrium concentration of Pb^{2+} . All analysis was conducted in triplicate and values are expressed as mean \pm SD.

2.7. Kinetic Models

To determine the absorption kinetics, 100 mL of aqueous solution containing 100 ppm of Pb^{2+} was taken in each of eighteen conical flasks. 0.05 g of resin was added in each flask. The conical flasks were shaken on wrist shaker (Burrell Scientific, Pittsburgh, PA, USA) for different time intervals at 303 K. The samples thus obtained were centrifuged at 3000 rpm for 15 min, filtered and analyzed using ICP-OES to get the residual concentration of Pb^{2+} in aqueous solution. All analysis was conducted in triplicate and values are expressed as mean \pm SD.

2.7.1. Pseudo-First-Order Kinetic Equation

The pseudo-first-order kinetic Equation (3), describes the adsorption of a Pb^{2+} from the aqueous solution [27]:

$$\frac{dq_t}{dt} = K_1(q_e - q_t) \quad (3)$$

where q_t is the amounts of Pb^{2+} adsorbed (mmol/g) at time t , $q_{e,1}$ is the amounts of Pb^{2+} adsorbed at equilibrium (mmol/g), and K_1 is the rate constant of pseudo-first-order adsorption process (min^{-1}). The linear form of Equation (3) is obtained after integration and application of the boundary conditions, and a plot of $\ln(q_e - q_t)$ versus t was used to compute the equilibrium adsorption capacity ($q_{e,cal}$), and adsorption rate constant (K_1).

2.7.2. Pseudo-Second-Order Kinetic Model

The pseudo-second-order kinetic model is based on the assumption that the rate of adsorption is proportional to the square of the difference in the equilibrium concentration of Pb^{2+} , mathematically expressed in Equation (4) [28]:

$$\frac{dq_t}{dt} = K_2(q_e - q_t)^2 \quad (4)$$

where K_2 (g/mg·min) is the equilibrium rate constant of pseudo-second-order adsorption. After applying the boundary conditions on Equation (4), a plot of the t/q_t versus t was used to compute the equilibrium adsorption capacity ($q_{e,cal}$) and adsorption rate constant (k_2).

2.7.3. Elovich Equation

Elovich's equation (Equation (5)) describes activated adsorption, which is compatible to with heterogeneous system [29].

$$\frac{dq_t}{dt} = \alpha \exp(-\beta q_t) \quad (5)$$

where α is the initial Pb^{2+} sorption rate [mmol/(g min)], and the parameter β is related to the extent of surface coverage and activation energy for chemisorption (g/mmol). After applying boundary conditions and integrating, the constants (β) and (α) can be obtained from the slope and intercept of the linear plot of q_t versus $\ln t$, respectively.

2.7.4. Intra-Particle Diffusion Equation

According to Weber and Morris [30], the intraparticle-diffusion kinetic model was employed to confirm particle diffusion within the bio-sorption system (Equation (6)):

$$q_t = K_{int}t^{0.5} + C \quad (6)$$

where K_{int} is the intra-particle diffusion constant (mg/g min^{1/2}). A linear plot of q_t versus $t^{0.5}$ was used to compute the constants C and K_{int} .

2.8. Adsorption Isotherms

The sorption isotherms were determined by adding 0.5 g of resin into a 250 mL volumetric flask containing Pb^{2+} ion (100 mL, 100 mg/L), with constant agitation at 120 rpm on a wrist shaker for 180 min at a controlled temperature. At the end of the sorption process, 5 mL of the sample was centrifuged at 3000 rpm for 15 min, and the Pb^{2+} concentration was determined using ICP-OES.

2.8.1. Langmuir Adsorption Isotherm

The Langmuir adsorption isotherm is based on the assumption that there are fixed numbers of equal size and shaped adsorption sites and dynamic equilibrium exists between the adsorbed and the free Pb^{2+} on the surface of the resin [31] Equation (7):

$$q_e = \frac{Q_0 k_L C_e}{1 + k_L C_e} \quad (7)$$

where Q_0 is the maximum monolayer coverage capacity (mg/g) and k_L is the Langmuir isotherm constant (L/mg). The values of the constants, $1/k_L$ and a_L/k_L can be estimated from the intercept and gradient from the plot of C_e/q_e versus C_e .

2.8.2. Dubinin-Radushkevich (D-R) Adsorption Isotherm

The Dubinin-Radushkevich isotherm describes the adsorption mechanism with a Gaussian energy distribution onto the resin surface [32] as expressed in Equation (8):

$$q_e = q_m e^{-\beta(RT \ln(1 + \frac{1}{C_e}))^2} \quad (8)$$

where q_m is monolayer adsorption capacity of Dubinin–Radushkevich (mg/g), β is adsorption energy E , R is the gas constant (8.314 J/mol K), and T is the absolute temperature. The constant β is computed from the relationship in Equation (9) [33]:

$$\beta = \frac{1}{2E^2} \quad (9)$$

The linear isotherm plot of $\ln q_e$ against $RT\left(1 + \frac{1}{C_e}\right)$ of Equation (9) gives q_m , as the intercept.

2.8.3. Temkin Adsorption Isotherm

Temkin isotherm considers the indirect Pb^{2+} – Pb^{2+} interactions on adsorption isotherms, as expressed by the generalized form, Equation (10) [34]:

$$q_e = \frac{RT}{B_T} \ln A_T C_e \quad (10)$$

where A_T is the Temkin isotherm equilibrium binding constant (L/g), B_T is the Temkin isotherm constant. Therefore, the plot of q_e versus $\ln C_e$ gives an intercept $\ln A_T$ and a straight line of slope RT/B_T .

2.8.4. Freundlich Adsorption Isotherm

Freundlich isotherm gives the empirical relationship between the concentration of Pb^{2+} on the surface of the resin to the concentration of Pb^{2+} in the aqueous solution, mathematically expressed as in Equation (11) [35]:

$$q_e = K_F C_e^{\frac{1}{n}} \quad (11)$$

where K_F is the Freundlich constant (mg/g), and n is the Freundlich exponent. The values of the constants, K_F and n can be estimated from the intercept and gradient from the plot of $\ln q_e$ versus $\ln C_e$.

3. Results and Discussion

3.1. Yield of Extracted Tannins and Resins per Gram of the Aqueous Fraction

The quantitative evaluation of the tannins and resins showed a significant variation ($p \leq 0.05$) in the content of the three different *Acacia* species, with ST and BT comparatively higher in tannin contents (Figure 3).

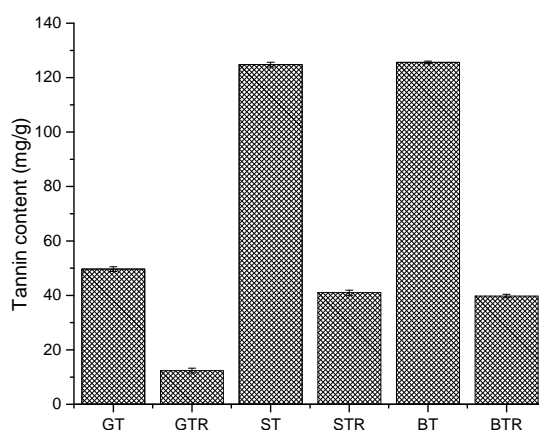


Figure 3. Comparative Yields of Extracted Tannins and Resins Expressed as Mean \pm SD. **Key:** silver wattle tannin (ST), silver wattle tannin resin (STR), black wattle tannin (BT), black wattle tannin resin (BTR), green wattle tannin (GT) and green wattle tannin resin (GTR).

There is a significant difference ($p \leq 0.05$) in the amount of cross-linkable tannin and extractable tannin; this indicates a difference in the tannin chemistry resulting in the observed variation.

Depending on the *Acacia* species, about 25–40% of the total tannin can be modified into a resin while the uncross-linkable tannin can still find application in the tanning industry [36,37].

3.2. Thermal and Functional Group Properties of the Tannins and Resins

The thermogravimetric plots of the tannins and resins are provided as Supplementary Materials (Figures S1–S3). The first weight loss of the extracted tannins and resins is attributed to the loss of moisture in a single step around 303–328 K and 380–384 K, with the highest loss being observed in GT (7%) and GTR (11%), respectively. According to Sepe [38], almost every resin contains some degree of absorbed atmospheric moisture which may influence the mechanical performance [39], and also the rate of absorption of the material [40].

There was a significant weight loss for all the extracted tannins at 328–384 K whereas the resins were thermally stable at 375–1020 K. This is an indication that the resins are more resilient to heat because of the inter- and intra-crosslinked functional groups which agrees with the observed differences in the FT-IR spectra of the tannins and corresponding resins (Figures S4–S6, Supplementary Materials).

The FT-IR spectra of the tannins and resins indicate the presence of O-H vibrations at 3248–3266 cm^{-1} . In addition, N-H vibration peaks at 3661–3669 cm^{-1} , C = C of aromatic and overtone patterns at 690–900 cm^{-1} were observed in spectra of the resins only. These vibrational frequencies confirm a successfully crosslinked and aromatic bridged resin [41,42]. After adsorption of Pb^{2+} , there was a shift in the vibrational peak positions, justifying the feasibility of the adsorption process.

3.3. Crystalline and Amorphous Profiling of the Tannins and Resins

The XRD patterns of the extracted tannins were used as references to changes in the pattern or peak position of resins (Figures S7–S9, Supplementary Materials). The diffractograms of GTR, BTR, and STR, revealed sharp diffraction peaks, corresponding to the crystalline region of tannins [43,44]. Crystalline peaks were observed to superimpose the broad amorphous background in all the diffractograms obtained in this study. Hence, the cross-linked resins have an improved crystalline character compared to their corresponding tannins. Additionally, peaks (2θ angle [intensity]) were observed on the diffractograms of the resins at 90.8° [446] for GTR, 90.9° [699], 108.3° [260], 114.1° [281] for STR and 88.9° [470] 100.9° [1891], 107.9° [127] for BTR. These variations in the XRD peaks may play an influential role in the sorption potential of the resins due to the creation of additional active sites [45].

3.4. Surface Morphology, Area and Pore Volume Analysis of the Resins

The surface morphology of the resins was examined using SEM-SE (JSM-7500F, Waltham, MA, USA) at a working distance of 8.1 mm at a thickness of 10 μm taken at different magnifications (Figure 4a–f). The micrographs of GTR and BTR have a porous, homogeneous, and crystallite morphology different from the broad heterogeneous surface of STR (Table 1).

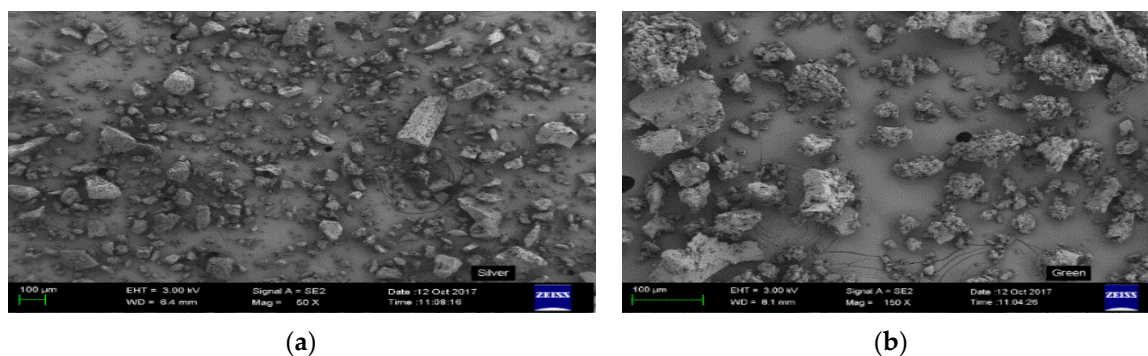


Figure 4. Cont.

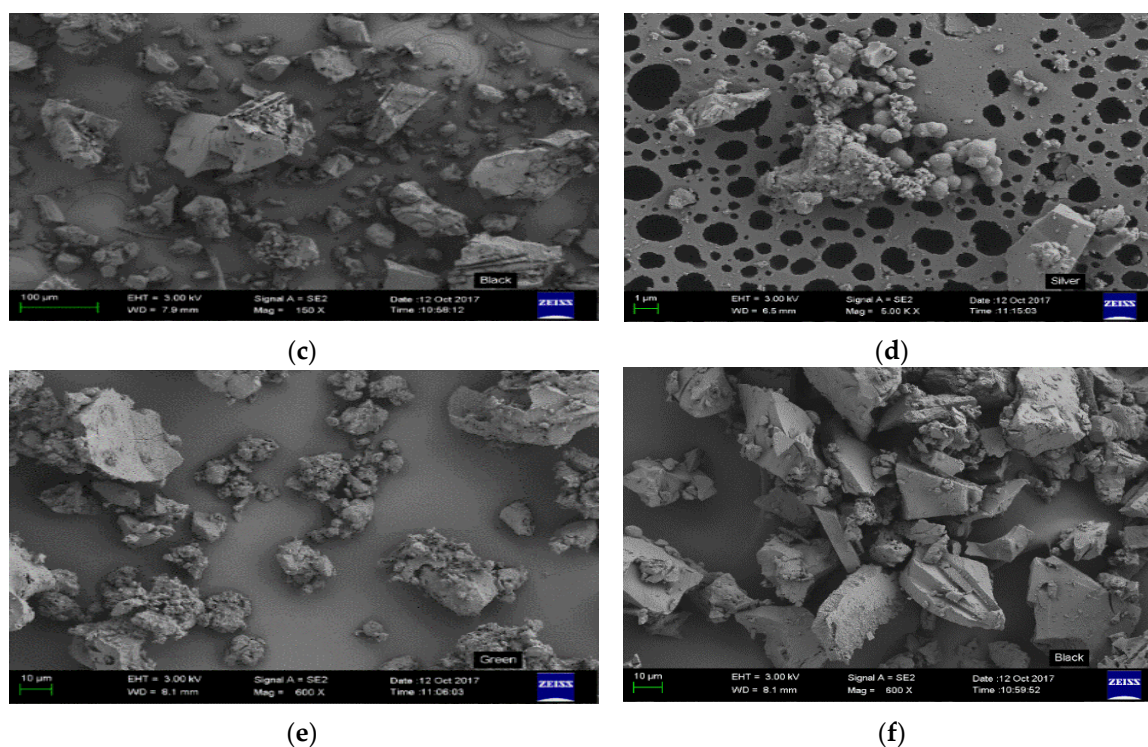


Figure 4. (a–f) Micrographs taken in SE mode at a magnification of $50\times$ for (a) STR (b) GTR and (c) BTR samples. Magnification of $600\times$ for (d) STR (e) GTR and (f) BTR samples.

There were no observable differences in the surface area as well as the pore volume of BTR and GTR (Table 1). The surface area is by no means the only physical property which determines the extent of adsorption. Of equal importance is the pore volume of the material. Mangun et al. [46] emphasized the importance of pore volume and area on the adsorption capacity of materials with heterogeneous surface compared to adsorbents with homogeneous surfaces.

Table 1. BET specific surface areas and pore volume for the resins.

| Synthesized Resin | Surface Area (m^2/g) | Pore Volume (cc/g) |
|-------------------|--|--------------------------------------|
| GTR | 2.38 | 9×10^{-3} |
| STR | 8.65 | 7×10^{-3} |
| BTR | 2.31 | 9×10^{-3} |

3.5. pH and Temperature Dependence of the Resins on Pb^{2+} Uptake

The uptake of Pb^{2+} by the resins was affected by variation in pH (Figure 5). STR has the best potential to accommodate the Pb^{2+} , efficiently removing over 74% of the ion from aqueous solutions at pH 6. There was a rapid increase in the adsorption of Pb^{2+} at pH 3.0, which peaks between pH 5 and 6 but drops off at pH 7. The adsorption of Pb^{2+} at pH 2–3 is low due to the competition between H_3O^+ and Pb^{2+} for the free poly-hydroxyl and amine groups on the resin, resulting in the limited number of binding sites available for the adsorption of Pb^{2+} .

The Pb^{2+} is precipitated at pH greater than 7, because of the high concentration of hydroxide ion and the ease of oxidizing the free poly-hydroxyl groups of the resins; hence the difficulty in evaluating the sorption capacity at higher pH. A similar observation has been reported by Liao et al. [47], where the adsorption could not be evaluated at $\text{pH} \geq 8.0$.

The influence of temperature on the adsorption of Pb^{2+} by the resins was significant ($p \leq 0.05$) (Table 2). As the temperature increases, the adsorption of Pb^{2+} gradually rises to a maximum at 294–328 K and drops off sharply at higher temperatures.

The electrostatic and exothermic nature of Pb^{2+} interaction with the resins was altered at a temperature > 328 K, despite the thermal stability of the resins above this temperature as shown on the thermograms (Figures S1–S3, Supplementary Materials). The observed decrease in the quantity of Pb^{2+} adsorbed at temperature > 328 K is evidence of the exothermic interaction of Pb^{2+} with the resin surface [48] and also the validity of the thermodynamic constant of Pb^{2+} at 288–300 K resulting in process reversal as reported in the studies of Seward [49] and Luo and Yanxin [50].

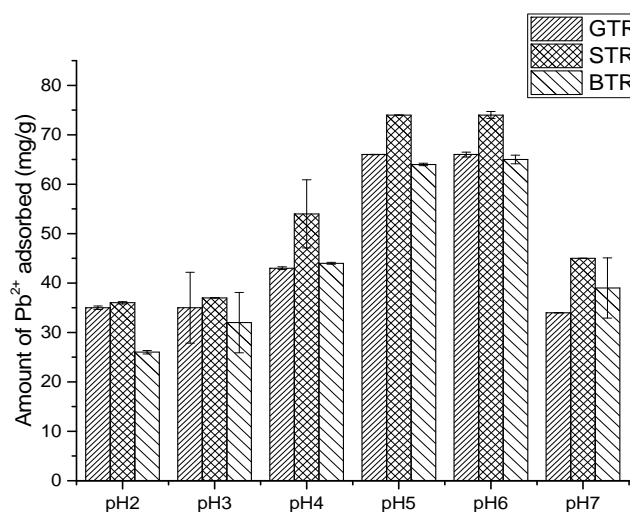


Figure 5. Effects of pH on the Pb^{2+} adsorption on the resins at an initial concentration of 100 ppm and powder resin concentration of 0.5 g/L (particle size + 100 μ m; agitation rate: 120 rpm; contact time: 180 min). Values are expressed as mean \pm SD.

Table 2. Effects of temperature on the Pb^{2+} adsorption on the resins at an initial concentration of 100 ppm (Resin: 0.5 g/L; particle size + 100 μ m; agitation rate: 120 rpm; contact time: 180 min).

| Resins | Optimal Temperature (K) | Amount of Pb^{2+} Absorbed (mg/g) |
|--------|-------------------------|-------------------------------------|
| STR | 328 | 81.65 |
| BTR | 294 | 69.96 |
| GTR | 294 | 66.18 |

3.6. Evaluation of Kinetics Results

In Figure 6, the Pb^{2+} uptake by the three resins with time responded linearly with a maximum removal at 180 min. To investigate the optimal rate-controlling step, kinetic experiments were performed at pH 6 for 180 min. Several kinetic models such as the pseudo-first-order, pseudo-second-order, Elovich model and inter-particle diffusion model were evaluated with their constants K_1 (1/min), K_2 (g/mg min) K_{int} (mg/g min^{1/2}), and α (mg/g min) computed from the graphs of the kinetic models. The kinetic plots of the resins are provided as Supplementary Materials (Figure S10a–d).

As seen in Table 3, the correlation coefficients obtained for the pseudo-second-order kinetic model has the highest r^2 value and was >0.95 of all resin interactions with Pb^{2+} . The theoretical $q_{e,cal}$ values of the pseudo-second-order model is closest to the experimental $q_{e,exp}$, even though its observed that the $K_1 > K_2$ at 303 K as a result of the exothermic nature of the interaction of Pb^{2+} with the resin causing a slight shift in equilibrium towards desorption. Similar kinetic behaviors using *Mimosa* tannin, carbon nanotubes and ethylenediamine-*N,N'*-disuccinic acid for the removal of Pb^{2+} were reported in the studies of Luzardo et al. [51] and Fabbricino et al. [52].

A suitable tool in evaluating the mechanistic evidence on a highly heterogeneous adsorbent is the Elovich equation. However, the observation in this study is contrary to the report of Aharoni and Ungarish [53], which stated that the Elovich equation should provide an excellent description of the

sorption of a divalent adsorbate provided it is entirely a chemisorption process. This implies that the sorption process in this study is not entirely an electrostatic process, as the computed value of the Dubinin–Radushkevich adsorption energy ($E \leq 7.07$ KJ/mol with a correlation coefficient > 0.9832 [54].

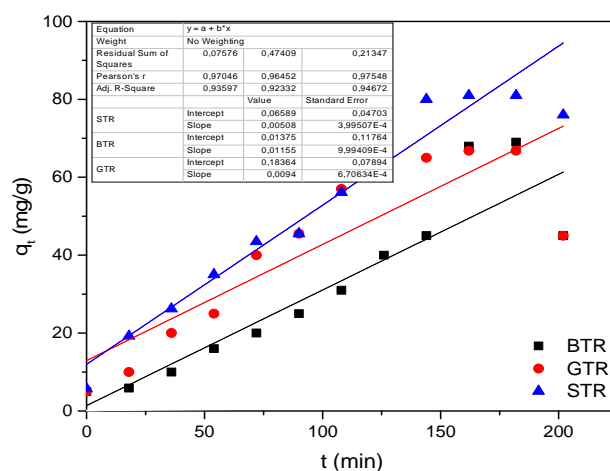


Figure 6. Plot of the equilibrium quantity of Pb^{2+} adsorbed with response to time by the three resins.

Table 3. The kinetics constants for the adsorption of Pb^{2+} (Resin: 0.5 g/L; C_i : 100 ppm; particle size + 100 μ m; temperature: 303 K; agitation rate: 120 rpm; contact time: 180 min; pH 6.

| Resins | $q_{e,exp}$ (mg/g) | Pseudo-First-Order Equation | | | Pseudo-Second-Order Equation | | |
|--------|--------------------|-----------------------------|--------------------|-------|--------------------------------------|--------------------|-------|
| | | K_1 (1/min) | $q_{e,cal}$ (mg/g) | r^2 | K_2 (g/mg min) | $q_{e,cal}$ (mg/g) | r^2 |
| STR | 93.37 | 0.067 | 10.63 | 0.966 | 0.055 | 93.87 | 0.953 |
| BTR | 83.43 | 0.073 | 68.36 | 0.853 | 0.042 | 84.64 | 0.958 |
| GTR | 63.74 | 0.063 | 52.27 | 0.912 | 0.074 | 64.83 | 0.983 |
| Resins | $q_{e,exp}$ (mg/g) | Elovich Equation | | | Intraparticle-Diffusion Equation | | |
| | | α (mg/g min) | β (g/min) | r^2 | K_{int} (mg/g min ^{1/2}) | r^2 | |
| STR | 73.37 | 5.363 | 6.323 | 0.993 | 0.367 | 0.983 | |
| BTR | 65.34 | 6473 | 3.345 | 0.835 | 0.647 | 0.783 | |
| GTR | 53.62 | 356.7 | 2.566 | 0.543 | 0.326 | 0.823 | |

In addition, the correlation coefficients obtained from the intra-particle diffusion model has a $r^2 \leq 0.98$ and an intercept at the origin for all the resins confirming Pb^{2+} diffusion within the system. This implies an increase in the boundary thickness for all resins [55], resulting in a decrease in the diffusion rate with time at a pH 6 due to limited active sites left on the resins at equilibrium.

3.7. Evaluation of the Isotherm Results

The equilibrium amount of Pb^{2+} effectively removed in 180 min by BTR was highest compared to STR and GTR (Figure 7). Hence, it is mandatory to determine the most suitable correlation model for the equilibrium data, to optimize the removal of Pb^{2+} from aqueous solutions. To accomplish the optimization requirements, we evaluated four isotherm models, determined the constants from the linear plots and the correlation coefficients (Table 4 and Figure S11a–d, Supplementary Materials).

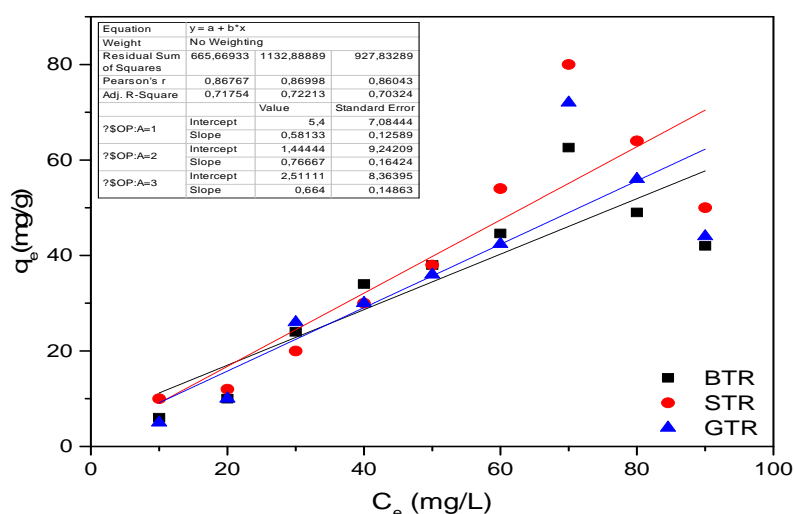
As seen in Table 4, high r^2 values were obtained from all isotherms, whereas the highest and lowest values were shown by Langmuir and Freundlich isotherms with 0.9966 and 0.7865, respectively. The Freundlich exponent (n) are all > 1 , an indication that the biosorption processes on all the resins are spontaneous [56]. Hence, it can be inferred that the resins are suitable for the removal of Pb^{2+} from aqueous solutions.

The adsorption mean-free energy (E) computed from the Dubinin–Radushkevich equation for the transfer of Pb^{2+} from the aqueous solution to the surface of the resin was found to be ≤ 7.07 KJ/mol. Consequentially, the mechanism of the adsorption of Pb^{2+} to the surface of the resin is partly a physical process as the mean-free energy is < 8 kJ/mol, as reported by Onyang et al. [54].

Table 4. Comparison of four isotherm equations for equilibrium uptake studies of Pb^{2+} by the three resins.

| Resins | Langmuir | | | | Dubinin–Radushkevich | | | |
|--------|-------------|--------------|--------------|--------|----------------------|---|--------------|--------|
| | K_L (L/g) | a_L (L/mg) | Q_0 (mg/g) | r^2 | q_m (mmol/g) | fi (mmol ² /J ²) | E (KJ/mol) | r^2 |
| STR | 37.84 | 0.326 | 189.30 | 0.9966 | 465.40 | 1×10^{-4} | 2.24 | 0.9744 |
| BTR | 13.98 | 0.363 | 105.70 | 0.9937 | 746.50 | 1×10^{-4} | 2.24 | 0.9367 |
| GTR | 11.83 | 0.464 | 98.82 | 0.9832 | 582.30 | 1×10^{-5} | 7.07 | 0.9543 |

| Resins | Temkin | | | Freundlich | | |
|--------|--------|-------------|--------|-----------------------------------|-------|--------|
| | B_T | A_T (L/g) | r^2 | K_F (mg/g)(mg/L) ^{1/n} | n | r^2 |
| STR | 14.74 | 127.60 | 0.9655 | 87.38 | 7.773 | 0.7865 |
| BTR | 10.73 | 32.32 | 0.9561 | 64.88 | 6.237 | 0.8853 |
| GTR | 2.83 | 45.37 | 0.9533 | 53.73 | 7.467 | 0.8335 |

**Figure 7.** Plot of the equilibrium quantity of Pb^{2+} adsorbed with response to concentration by the three resins.

The Temkin isotherm ($r^2 = 0.95$) indicates that the adsorption fits the electrostatic model of Pb^{2+} — Pb^{2+} interaction at the resin interface. As the low Temkin constant (B_T) values are 2.83–14.74 gJ/mg·mol for the indirect Pb^{2+} — Pb^{2+} interactions with resin interface, this indicates an exothermic adsorption process leading to a decrease in the amount of Pb^{2+} adsorbed as temperature increases [57].

4. Conclusions

This study showed that the removal of Pb^{2+} from aqueous solutions in a batch system using resins from invasive *Acacia* species is an effective and feasible method. The resins were found to have improved crystalline property, high thermal stability, additional chemical functionality, and pronounced immobilization properties. In addition to these features, the uniquely small pore volume of $7\text{--}9 \times 10^{-3}$ cc/g, with large surface area, enhanced the adsorption capacity of the resins. Temperature and pH strongly influenced the adsorption capacity of Pb^{2+} by the resins. Adsorption equilibrium data revealed that there are two sorption processes taking place on the surface of the resins with the dominant driving force being chemisorption. From a thorough literature survey as well as the result from this study, the resins may be used as an effective adsorbent for the removal of Pb^{2+} in aqueous solutions. They are less expensive, more easily synthesized and do not require any form of activation as in the case of some commercial adsorbents. The resins are attractive not only from an economic point of view but also for the environmental impact of reducing and recovering invasive plant material. Therefore, the properties of this resin must be considered when making a valuable group of novel commercial adsorbents.

Supporting Information: Including thermograms, micrographs, diffractograms and FT-IR spectra of STR, BTR and GTR are available as supplementary material.

Supplementary Materials: The following are available online at <http://www.mdpi.com/2073-4441/10/5/648/s1>.

Author Contributions: Conceptualization, Johannes S. Modise and Bamidele J. Okoli; Methodology, Bamidele J. Okoli and Gabriel O. Anyanwu; Software, Bamidele J. Okoli and Johannes S. Modise; Validation, Bamidele J. Okoli and Gabriel O. Anyanwu and Johannes S. Modise; Formal Analysis, Johannes S. Modise; Investigation, Patience M. Shilowa and Bamidele J. Okoli; Resources, Johannes S. Modise; Data Curation, Gabriel O. Anyanwu and Bamidele J. Okoli; Writing-Original Draft Preparation, Patience M. Shilowa and Bamidele J. Okoli; Writing-Review & Editing, Bamidele J. Okoli and Gabriel O. Anyanwu; Visualization, Gabriel O. Anyanwu.; Supervision, Johannes S. Modise; Project Administration, Johannes S. Modise; Funding Acquisition, Johannes S. Modise.

Funding: This research received no external funding.

Acknowledgments: We appreciate the Institute of Chemical and Biotechnology, Faculty of Applied and Computer Science Research, Vaal University of Technology, South Africa, for supporting the research.

Conflicts of Interest: The authors have declared that there is no conflict of interest.

Abbreviations

| | |
|---------|--|
| XRD | X-ray Diffractometer |
| BET | Brunauer–Emmett–Teller |
| TGA | Thermogravimetric analyzer |
| SEM | Scanning electron microscopy |
| FT-IR | Fourier transform infrared spectroscopy |
| ST | Silver Wattle Tannin |
| BT | Black Wattle Tannin |
| GT | Green Wattle Tannin |
| STR | Silver Wattle Tannin Resin |
| GTR | Green Wattle Tannin Resin |
| BTR | Black Wattle Tannin Resin |
| ICP-OES | Inductively coupled plasma optical emission spectrometer |
| * | After adsorption |

References

- Bharti, N.; Katyal, D. Water quality indices used for surface water vulnerability assessment. *J. Environ. Sci.* **2011**, *2*, 154–173. [[CrossRef](#)]
- Manara, A. Plants and heavy metals. *Signal Transduct.* **2012**, 27–54. [[CrossRef](#)]
- Agência Nacional das Águas (ANA). *Cuidando das águas: Soluções para melhorar a qualidade dos recursos hídricos*; Agência Nacional das Águas (ANA): Brasília, Brazil, 2011; ISBN 978-85-8210-018-9. (In Portuguese)
- Duse, A.G.; Da Silva, M.P.; Zietsman, I. Coping with hygiene in South Africa, a water scarce country. *Int. J. Environ. Health Res.* **2003**, *13* (Suppl. 1), S95–S105. [[CrossRef](#)] [[PubMed](#)]
- Chamier, J.; Schachtschneider, K.; le Maitre, D.C.; Ashton, P.J.; van Wilgen, B.W. Impacts of invasive alien plants on water quality, with particular emphasis on South Africa. *Water SA* **2012**, *38*, 345–356. [[CrossRef](#)]
- Calder, I.R.; Dye, P. Hydrological impacts of invasive alien plants. *Land Use Water Resour. Res.* **2001**, *1*, 1–8.
- Görgens, A.H.M.; Van Wilgen, B.W. Invasive alien plants and water resources in South Africa: Current understanding, predictive ability and research challenges. *S. Afr. J. Sci.* **2004**, *100*, 27–33.
- Wells, M.J.; Balsinhas, A.A.; Joffe, H.; Engelbrecht, V.M.; Harding, G.; Stirton, C.H. A catalogue of problem plants in Southern Africa. In *Catalogue of Problem Plants in Southern Africa*; Botanical Research Institute: Lucknow, India, 1986.
- Dogra, K.; Sood, S.; Dobhal, P.; Seema, S. Alien plant invasion and their impact on indigenous species diversity at global scale: A review. *J. Ecol. Nat. Environ.* **2010**, *2*, 175–186.
- Anoop Krishnan, A.; Anirudhan, T.S. Removal of lead(II) in the presence of organic ligand from aqueous solution using activated carbon. *Indian J. Environ. Prot.* **2002**, *22*, 52–59.

11. Issabayeva, G.; Aroua, M.K.; Sulaiman, N.M.N. Removal of lead from aqueous solutions on palm shell activated carbon. *Bioresour. Technol.* **2006**, *97*, 2350–2355. [[CrossRef](#)] [[PubMed](#)]
12. Nriagu, J.O. Lead orthophosphates. I. Solubility and hydrolysis of secondary lead orthophosphate. *Inorg. Chem.* **1972**, *11*, 2499–2503. [[CrossRef](#)]
13. Can, M.; Bulut, E.; örnek, A.; özacar, M. Synthesis and characterization of Valonea tannin resin and its interaction with palladium (II), rhodium (III) chloro complexes. *Chem. Eng. J.* **2013**, *221*, 146–158. [[CrossRef](#)]
14. Bin, Z.; Shawon, Z. Synthesis and characterization of janus magnetic nanoparticles and its application as an adsorbent. *J. Chem. Eng.* **2012**, *27*, 64–68.
15. Peres, R.S.; Armelin, E.; Alemán, C.; Ferreira, C.A. Modified tannin extracted from black wattle tree as an environmentally friendly antifouling pigment. *Ind. Crops Prod.* **2015**, *65*, 506–514. [[CrossRef](#)]
16. Zhao, C.; Zheng, H.; Sun, Y.; Liu, B.; Zhou, Y.; Liu, Y.; Zheng, X. Fabrication of tannin-based dithiocarbamate biosorbent and its application for Ni(II) Ion removal. *Water. Air Soil Pollut.* **2016**, *228*. [[CrossRef](#)]
17. Binaeian, E.; Seghatoleslami, N.; Chaichi, M.J. Synthesis of oak gall tannin-immobilized hexagonal mesoporous silicate (OGT-HMS) as a new super adsorbent for the removal of anionic dye from aqueous solution. *Desalin. Water Treat.* **2016**, *57*, 8420–8436. [[CrossRef](#)]
18. Karamać, M. Fe(II), Cu(II) and Zn(II) chelating activity of buckwheat and buckwheat tannin groats tannin fractions. *Polish J. Food Nutr. Sci.* **2007**, *57*, 357–362.
19. Karamać, M. Chelation of Cu(II), Zn(II), and Fe(II) by tannin constituents of selected edible nuts. *Int. J. Mol. Sci.* **2009**, *10*, 5485–5497. [[CrossRef](#)] [[PubMed](#)]
20. Santana Romero, J.L.; Martínez Luzardo, F.; Codorníu Hernández, E.; Vargas Guerra, L.; Melo Cala, P.; García Guillén, M.; Isaac Olivé, K.; Estevez, P.; Roque Córdoba, A.; Benítez, M. Radioisotope method for characterization of vegetable tannins, extracted from waste of forestry production in Cuba. *J. Radioanal. Nucl. Chem.* **2002**, *253*, 101–106. [[CrossRef](#)]
21. Liao, X.; Zhang, M.; Shi, B. Collagen-fiber-immobilized tannins and their adsorption of Au(III). *Ind. Eng. Chem. Res.* **2004**, *43*, 2222–2227. [[CrossRef](#)]
22. Chibata, I.; Tosa, T.; Mori, T.; Watanabe, T.; Sakata, N. Immobilized tannin—A novel adsorbent for protein and metal ion. *Enzym. Microb. Technol.* **1986**, *8*, 130–136. [[CrossRef](#)]
23. Bamidele, O.; Nnana, M.; Imelda, L.; Sekomeng, M. Acacia decurrens (wild) an invasive South Africa tree: Chemical profile, antibacterial and antioxidant activities. *Org. Med. Chem. IJ* **2017**, *3*. [[CrossRef](#)]
24. Guillemaud, T.; Ciosi, M.; Lombaert, É.; Estoup, A. Biological invasions in agricultural settings: Insights from evolutionary biology and population genetics. *C.R. Biol.* **2011**, *334*, 237–246. [[CrossRef](#)] [[PubMed](#)]
25. Kaur, C.; Kapoor, H.C. Anti-oxidant activity and total phenolic content of some Asian vegetables. *Int. J. Food Sci. Technol.* **2002**, *37*, 153–161. [[CrossRef](#)]
26. Shirato, W. Method of Preparing Insoluble Hydrolysable Tannin and Method of Treating Waste Liquid with the Tannin. U.S. Patent 5,274,169, 28 September 1993.
27. Ho, Y.S.; McKay, G. A Comparison of chemisorption kinetic models applied to pollutant removal on various sorbents. *Process Saf. Environ. Prot.* **1998**, *76*, 332–340. [[CrossRef](#)]
28. Ho, Y.-S. Removal of copper ions from aqueous solution by tree fern. *Water Res.* **2003**, *37*, 2323–2330. [[CrossRef](#)]
29. Cheung, C.W.; Porter, J.F.; McKay, G. Sorption kinetic analysis for the removal of cadmium ions from effluents using bone char. *Water Res.* **2001**, *35*, 605–612. [[CrossRef](#)]
30. Weber, W.J.; Morris, J.C. Kinetics of adsorption on carbon from solution. *J. Sanit. Eng. Div.* **1963**, *89*, 31–60.
31. Langmuir, I. Adsorption of gases on plain surface of glass mica platinum. *J. Am. Chem. Soc.* **1918**, *40*, 1361–1403. [[CrossRef](#)]
32. Dubinin, M.M.; Radushkevich, L.V. The equation of the characteristic curve of activated charcoal. *Proc. Acad. Sci. Phys. Chem. Sect.* **1947**, *55*, 331. [[CrossRef](#)]
33. Namasivayam, C.; Sureshkumar, M.V. Removal of chromium(VI) from water and wastewater using surfactant modified coconut coir pith as a biosorbent. *Bioresour. Technol.* **2008**, *99*, 2218–2225. [[CrossRef](#)] [[PubMed](#)]
34. Ho, Y.S.; Ng, J.C.Y.; McKay, G. Removal of lead(II) from effluents by sorption on peat using second-order kinetics. *Sep. Sci. Technol.* **2001**, *36*, 241–261. [[CrossRef](#)]
35. Freundlich, H. Über die adsorption in Lösungen. *Z. Phys. Chem.* **1907**, *57*, 385–470. [[CrossRef](#)]

36. Sieniawska, E.; Baj, T. Tannins. In *Pharmacognosy: Fundamentals, Applications and Strategy*; Elsevier: New York, NY, USA, 2016; pp. 199–232, ISBN 9780128020999.
37. Swanson, B.G. Tannins and polyphenols. In *Encyclopedia of Food Sciences and Nutrition*; Elsevier: New York, NY, USA, 2003; pp. 5729–5733, ISBN 9780122270550.
38. Sepe, M. Why (And What) You Need to Dry. *Plast. Technol.* 2014. Available online: <https://www.ptonline.com/articles/why-and-what-you-need-to-dry> (accessed on 23 April 2018).
39. Baschek, G.; Hartwig, G.; Zahradnik, F. Effect of water absorption in polymers at low and high temperatures. *Polymer* **1999**, *40*, 3433–3441. [[CrossRef](#)]
40. Ye, Z.B.; Cheng, L.; Xiang, W.T.; Liu, Y.G.; Li, J.H. Characterization of resins and the adsorption of resins on asphaltene particles. *Xinan Shiyou Daxue Xuebao/J. Southwest Pet. Univ.* **2010**, *32*, 147–154. [[CrossRef](#)]
41. Grabowska, B.; Holtzer, M. Structural examination of the cross-linking reaction mechanism of polyacrylate binding agents. *Arch. Metall. Mater.* **2009**, *54*, 427–437.
42. González-González, M.; Cabanelas, J.C.; Baselga, J. Applications of FTIR on epoxy resins – identification, monitoring the curing process, phase separation and water uptake. In *Infrared Spectroscopy-Materials Science, Engineering and Technology*; Theophile, T., Ed.; InTech: Rijeka, Croatia, 2012; Volume 2, pp. 261–284.
43. Almeida, E. Surface treatments and coatings for metals. A general overview. 1. Surface treatments, surface preparation, and the nature of coatings. *Ind. Eng. Chem. Res.* **2001**, *40*, 3–14. [[CrossRef](#)]
44. Narayanan, T.S.N. Surface pretreatment by phosphite conversion coatings—A review. *History* **2005**, *9*, 130–177.
45. Peres, R.S.; Cassel, E.; Ferreira, C.A.; Azambuja, D.S. Grain refiner effect of black wattle tannin in iron and zinc phosphate coatings. *Ind. Eng. Chem. Res.* **2014**, *53*, 2706–2712. [[CrossRef](#)]
46. Mangun, C.L.; Daley, M.A.; Braatz, R.D.; Economy, J. Effect of pore size on adsorption of hydrocarbons in phenolic-based activated carbon fibers. *Carbon* **1998**, *36*, 123–129. [[CrossRef](#)]
47. Liao, X.; Li, L.; Shi, B. Adsorption recovery of thorium(IV) by Myrica rubra tannin and larch tannin immobilized onto collagen fibres. *J. Radioanal. Nucl. Chem.* **2004**, *260*, 619–625. [[CrossRef](#)]
48. Dho, N.Y.; Lee, S.R. Effect of temperature on single and competitive adsorptions of {Cu} (II) and {Zn} (II) onto natural clays. *Environ. Monit. Assess.* **2003**, *83*, 177–203. [[CrossRef](#)] [[PubMed](#)]
49. Seward, T.M. The formation of lead (II) chloride complexes to 300 C: A spectrophotometric study. *Geochim. Cosmochim. Acta* **1984**, *48*, 121–134. [[CrossRef](#)]
50. Luo, Y.; Millero, F.J. Stability constants for the formation of lead chloride complexes as a function of temperature and ionic strength. *Geochim. Cosmochim. Acta* **2007**, *71*, 326–334. [[CrossRef](#)] [[PubMed](#)]
51. Luzardo, F.H.M.; Velasco, F.G.; Correia, I.K.S.; Silva, P.M.S.; Salay, L.C. Removal of lead ions from water using a resin of *Mimosa* tannin and carbon nanotubes. *Environ. Technol. Innov.* **2017**, *7*, 219–228. [[CrossRef](#)]
52. Fabbicino, M.; Ferraro, A.; Luongo, V.; Pontoni, L.; Race, M. Soil washing optimization, recycling of the solution, and ecotoxicity assessment for the remediation of Pb-contaminated sites using EDDS. *Sustainability* **2018**, *10*, 636. [[CrossRef](#)]
53. Aharoni, C.; Ungarish, M. Kinetics of activated chemisorptions. Part I: The non-elovichian part of the isotherm. *J. Chem. Soc. Faraday Trans.* **1976**, *72*, 265–268. [[CrossRef](#)]
54. Onyang, M.S.; Kojima, Y.; Aoyi, O.; Bernardo, E.C.; Matsuda, H. Adsorption equilibrium modeling and solution chemistry dependence of fluoride removal from water by trivalent-cation-exchanged zeolite F-9. *J. Interface Sci.* **2004**, *279*, 341–350. [[CrossRef](#)] [[PubMed](#)]
55. Hameed, B.H. Equilibrium and kinetic studies of methyl violet sorption by agricultural waste. *J. Hazard. Mater.* **2008**, *154*, 204–212. [[CrossRef](#)] [[PubMed](#)]
56. Hameed, B.H.; Mahmoud, D.K.; Ahmad, A.L. Equilibrium modeling and kinetic studies on the adsorption of basic dye by a low-cost adsorbent: Coconut (*Cocos nucifera*) bunch waste. *J. Hazard. Mater.* **2008**, *158*, 65–72. [[CrossRef](#)] [[PubMed](#)]
57. Sekar, M.; Sakthi, V.; Rengaraj, S. Kinetics and equilibrium adsorption study of lead(II) onto activated carbon prepared from coconut shell. *J. Colloid Interface Sci.* **2004**, *279*, 307–313. [[CrossRef](#)] [[PubMed](#)]

